JOURNAL OF Materials CHEMISTRY

Synthesis and crystal packing of large polycyclic aromatic hydrocarbons: hexabenzo[*bc*,*ef*,*hi*,*kl*,*no*,*qr*]coronene and dibenzo[*fg*,*ij*]phenanthro[9,10,1,2,3-*pqrst*]pentaphene

Christian Kübel, Karin Eckhardt, Volker Enkelmann, Gerhard Wegner and Klaus Müllen*

Max-Planck-Institut for Polymer Research, Ackermannweg 10, D-55128 Mainz, Germany; Fax. +49 6131 379 100. E-mail: muellen@mpip-mainz.mpg.de

Received 10th November 1999, Accepted 21st January 2000

A detailed study of the oxidative cyclodehydrogenation of two oligophenylene precursors resulting in large polycyclic aromatic hydrocarbons (PAHs) which contain up to 42 carbon atoms gave insight into the reaction course. This study confirmed that the reaction occurs exclusively in an intramolecular fashion without the formation of organic side products. X-Ray diffraction, selected area electron diffraction, and low-dose high-resolution electron microscopy were used to analyse the effect of heat treatment and sublimation on the morphology and crystal structure of large PAHs, hexabenzo[*bc*,*ef*,*hi*,*kl*,*no*,*qr*]coronene (HBC) and dibenzo[*fg*,*ij*]phenanthro[9,10,1,2,3-*pqrst*]pentaphene (DBPP). HBC crystallizes in the γ-motif, as has been determined from single crystals previously. The experiments showed that small crystals exhibit some characteristic distortions of the unit cell. DBPP also crystallizes also in the γ-motif, but due to the "double-bay area" in the periphery of the molecule channels with a diameter of about 4 Å are formed in the crystal.

Introduction

Polycyclic aromatic hydrocarbons (PAHs) have intensively been investigated since the pioneering works of Scholl,[1] Clar[2] and Zander.[3] Besides synthetic challenges, correlations between the chemical structure of PAHs and their electronic properties, as well as their packing behavior in the solid state, have been a key concern. Analysis of the electronic properties of small PAHs led to a better understanding of the electronic structure of aromatic systems.[4] Large PAHs can formally be regarded as two-dimensional graphite sub-units and are well defined model systems for graphite. Different theoretical methods have been applied to estimate the electronic properties of graphite based on PAHs with increasing size and varying topologies.[5] Large aromatic compounds also play a crucial role during the graphitation of organic compounds. PAHs with a diameter of 1–2 nm constitute the so-called basic structural units of the carbomesophase where they form a nematic discotic liquid crystalline phase, the key step for the formation of well ordered anisotropic graphitic structures.[6] In combination with the relatively simple molecular structure this has stimulated research to gain an improved understanding of the packing behavior of such compounds. It led to a rationalization of four typical herringbone-type structures for PAHs.[7] An interesting question in this regard is whether a transition to a planar, graphitic structure will occur if the diameter of the PAH increases and at which size this will be observed.

Intramolecular oxidative cyclodehydrogenation of oligophenylene precursors, which has recently been described,[8] gives access to extremely large PAHs, which could eventually lead to a further understanding of graphitic materials and their electronic properties. Herein, the synthesis and packing behavior of two large polynuclear aromatic compounds, hexabenzo[*bc*,*ef*,*hi*,*kl*,*no*,*qr*]coronene (HBC) and dibenzo[*fg*,*ij*]-phenanthro[9,10,1,2,3-*pqrst*]pentaphene (DBPP) were analysed in order to develop improved processing methods for ultra-large PAHs. Next to their electronic role as molecular models of graphite, the compounds examined here, in particular DBPP, show some interesting structural features due to molecular shape as will be discussed below.

Results and discussion

Synthesis

Several pathways for the synthesis of hexa-*peri*-hexabenzocoronene (HBC) are described in the literature,[9] however oxidative cyclodehydrogenation of hexaphenylbenzene (**1**, HPB) with copper(II) chloride and aluminum(III) trichloride is the most convenient method (Scheme 1).[8] When using typical experimental conditions[8] the only product observed was HBC **3**, which was clearly identified by isotopically resolved field desorption-mass spectrometry (FD-MS). By using a smaller excess of the oxidizing agent intermediate products with two and four newly formed carbon–carbon bonds were also observed by FD-MS (Fig. 1). It was even possible to isolate phenyldibenzo[*fg*,*ij*]phenanthro[9,10,1,2,3-*pqrst*]pentaphene (**2**), which was formed in about 10% yield (see Experimental section). Other intermediate products containing only two new carbon–carbon bonds were observed in trace amounts.

Surprisingly, the solubility of compound **2** is even higher than that of the starting compound hexaphenylbenzene (**1**) and this enabled a detailed NMR-spectroscopic analysis. The ^{1}H–^{1}H COSY NMR spectrum of the intermediate reaction product **2** could be completely assigned and clearly confirmed the proposed structure for compound **2** (Fig. 2). Furthermore, NMR-spectroscopic analysis of the reaction mixture showed that compound **2** was the only partially cyclodehydrogenated species formed under the reaction conditions. The insoluble material was separated by filtration. No partially cyclodehydrogenated products were observed in the insoluble fraction by FD-mass spectrometry. In the soluble fraction the concentration of any other possible intermediate product other than compound **2** was below the detection limit of the NMR-spectroscopic measurement.

The observation and isolation of intermediate products proves that oxidative cyclodehydrogenation does not occur as a concerted planarization of all phenyl rings under carbon–carbon bond formation in one step, but proceeds in separate reaction steps. The fact that compound **2** was the only

DOI: 10.1039/a908941a

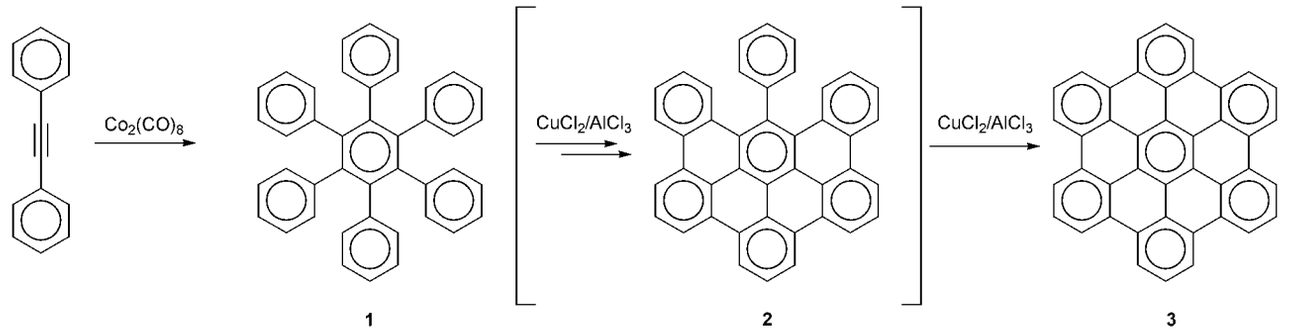

Scheme 1 Oxidative cyclodehydrogenation of hexaphenylbenzene[8] yielding HBC (**3**) after formation of an intermediate product **2**.

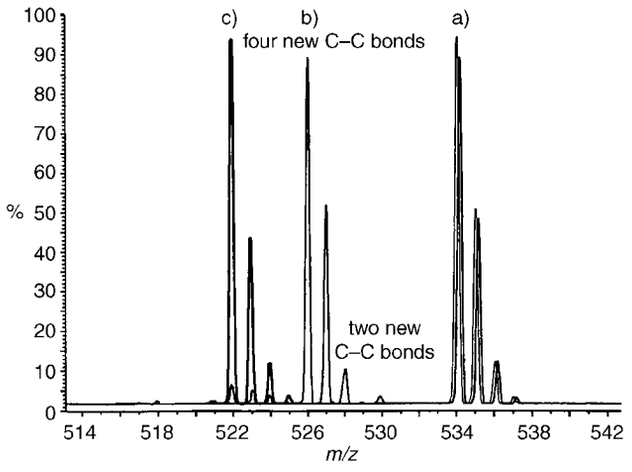

Fig. 1 Normalized superposition of FD-mass spectra taken at three different times during cyclodehydrogenation of HPB **1**: (a) Before the reaction (only HPB **1**), (b) after 12 h with 1.5 eq. of oxidizing agent per carbon–hydrogen bond (partially cyclodehydrogenated products, HPB **1** and small amounts of HBC **3**), (c) after two days with 3 eq. of $AlCl_3$ per carbon–hydrogen bond (only HBC).

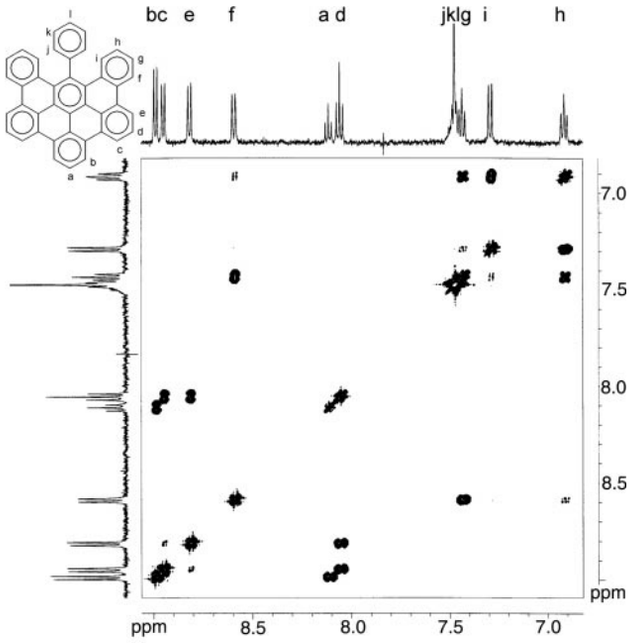

Fig. 2 ^1H–^1H NMR spectrum (500 MHz, 353 K, 1,1,2,2-tetrachloroethane-d_2) of phenyldibenzo[*fg*,*ij*]phenanthro[9,10,1,2,3-*pqrst*]pentaphene (**2**).

observable product upon quenching of the reaction, indicates that **2** is the most stable intermediate.

Further oxidation of the partially cyclodehydrogenated mixture by adding more oxidizing agent lead to the formation of HBC **3**. Owing to the low solubility, the final product, HBC **3**, could only be analysed by UV/Vis spectroscopy, which is in agreement with spectra published by Clar *et al.*,[9a] and by FD-MS as well as by LD-TOF-MS, which showed that no other organic by-products were formed. In particular, no dimers or higher oligomers of HBC were observed, indicating that cyclodehydrogenation occurs only intramolecularly, not intermolecularly. This is also in agreement with observations made during the synthesis of ultra-large PAHs.[8]

Dibenzo[*fg*,*ij*]phenanthro[9,10,1,2,3-*pqrst*]pentaphene (**5**) can be synthesized similarly to hexabenzo[*bc*,*ef*,*hi*,*kl*,*no*,*qr*]coronene (**3**) by oxidative cyclodehydrogenation of 1,2,3,4,5-pentaphenylbenzene (**4**) with copper(II) dichloride and aluminium(III) trichloride (Scheme 2). UV/Vis-spectroscopic analysis of the reaction product is in agreement with the spectrum of DBPP **5** published by Clar *et al.*[9a] In addition, we were able clearly to identify the product **5** by NMR spectroscopy and FD-mass spectrometry. In contrast to HBC **3**, the solubility of DBPP **5** in hot 1,1,2,2-tetrachloroethane is high enough to record a well resolved ^1H–^1H COSY NMR spectrum, which was completely assigned (Fig. 3). Note that proton a experiences a remarkably low-field shift to δ 10.36 as a result of the combined deshielding effect of the five neighboring benzene rings.

Coupling of two or more DBPP molecules due to intermolecular reactions was not observed by NMR spectroscopy or FD-mass spectrometry, which is again consistent with the assumption that the oxidative cyclodehydrogenation occurs only intramolecularly.

The optical properties of the partially cyclodehydrogenated product **2** and DBPP **5** are similar as expected for the same chromophore (Fig. 4). Nevertheless, this result is not trivial. Whereas DBPP **5** is a planar molecule, the partially cyclodehydrogenated product **2** should be strongly twisted as semiempirical AM1 calculations[10] show in agreement with the crystal structure of the structurally comparable 9,18-diphenyltetrabenz[*a*,*c*,*h*,*j*]anthracene (**6**)[11] (Fig. 5).

The energy barrier for the twist inversion of an isopropyl derivative of compound **6** was determined to be 16.7 kcal mol^{-1} by NMR spectroscopy,[11] which is comparable to the difference in heat of formation of about 15 kcal mol^{-1} for the symmetric planar and the twisted conformation of **2**. The NMR measurements for the isopropyl derivative of **6** show that the energy barrier is sufficiently low for the twist inversion to occur on the NMR timescale at 300 K,[11] suggesting a similarly high flexibility for compound **2**.

Crystal structures

The grain size of the material obtained after synthesis depends on the quenching conditions of the cyclodehydrogenation

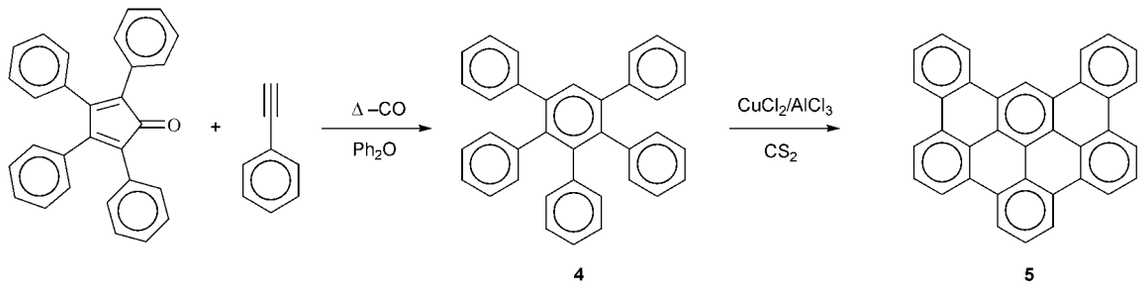

Scheme 2 Cyclodehydrogenation of pentaphenylbenzene[9] (**4**) resulting in dibenzo[*fg*,*ij*]phenanthro[9,10,1,2,3-*pqrst*]pentaphene (**5**).

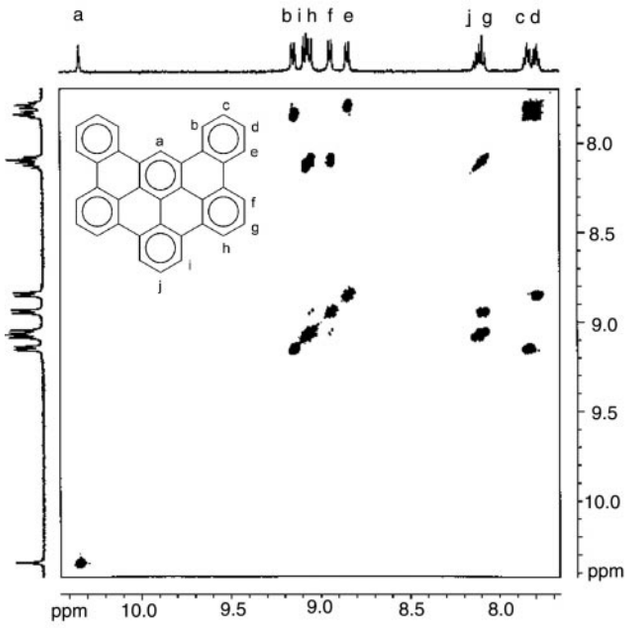

Fig. 3 ^{1}H–^{1}H NMR spectrum (500 MHz, 353 K, 1,1,2,2-tetrachloroethane-d_2) of dibenzo[*fg*,*ij*]phenanthro[9,10,1,2,3-*pqrst*]pentaphene (**5**).

reaction.[12] Scanning (SEM) and transmission electron microscopy (TEM) mainly show aggregates with an irregular shape (Fig. 6a). However, within these aggregates there are some small single crystals, which give rise to well defined diffraction patterns in selected area electron diffraction (SAED).[13] Fig. 6(b) shows a typical diffraction pattern of such a single crystal surrounded by nanocrystals.

The appearance of the electron diffraction pattern is very similar to that of the [001] zone of the single crystal structure of HBC **3** grown from molten pyrene by Goddard *et al.*,[14] which indicates a similar packing pattern for these relatively rapidly

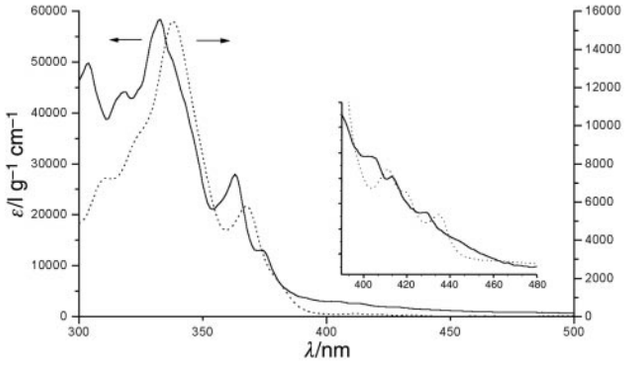

Fig. 4 UV/Vis spectra ($CHCl_3$) of phenyldibenzo[*fg*,*ij*]phenanthro[9,10,1,2,3-*pqrst*]pentaphene (**2**) (dotted line, right axis) and dibenzo[*fg*,*ij*]phenanthro[9,10,1,2,3-*pqrst*]pentaphene (**5**) (full line, left axis).

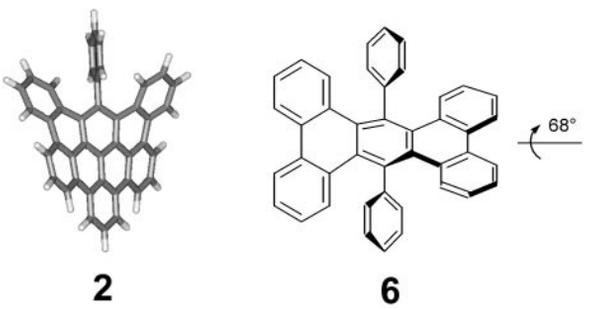

Fig. 5 Structure of phenyldibenzo[*fg*,*ij*]phenanthro[9,10,1,2,3-*pqrst*]pentaphene (**2**) according to AM1 calculations[10] (left) and sketch of the structure of 9,18-phenyltetrabenz[*a*,*c*,*h*,*j*]anthracene (**6**) according to crystal structure analysis[11] (right).

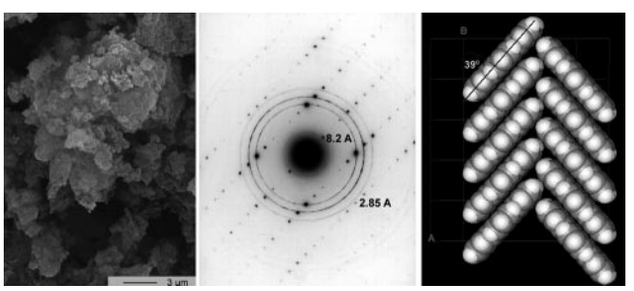

Fig. 6 (a) SEM micrograph of microcrystalline HBC **3** obtained directly after synthesis. (b) Selected area electron diffraction pattern of the [001] zone of a microcrystal of HBC **3** surrounded by some nanocrystals (same batch as in a). (c) Packing of HBC molecules along *b* direction.

precipitated microcrystals. However, a detailed analysis of the reciprocal spacings shows that the structure of the microcrystals is slightly distorted compared to the single crystal structure.[14] With the assumption of an interplanar spacing of 3.5 Å a tilt angle of 38° between the molecular plane and the stacking axis (5.7 Å from the reciprocal spacing of 1/2.85 $Å^{-1}$) can be calculated (Fig. 6c). This differs from the angle of 44°, which has been determined from the single crystal structure. Taking this tilt angle an interplanar spacing of about 3.9 Å results which is unreasonably large for a π–π stacking distance. This deviation is probably due to kinetic effects during fast precipitation of the HBC molecules.

One possibility to obtain highly crystalline samples or single crystals of PAHs is crystallization from pyrene or in some cases even from 1,2,4-trichlorobenzene solution at high temperatures.[14] However, we found it more convenient to grow single crystals of PAHs by heat treatment or sublimation under vacuum using a temperature gradient.[15]

When HBC **3** was annealed under nitrogen at 400 °C for 4 days large needle-shaped crystals which were up to 50 μm long formed from the microcrystalline aggregates. X-Ray powder diffraction and selected area electron diffraction (Fig. 7) showed that the material obtained was dominated by a crystal

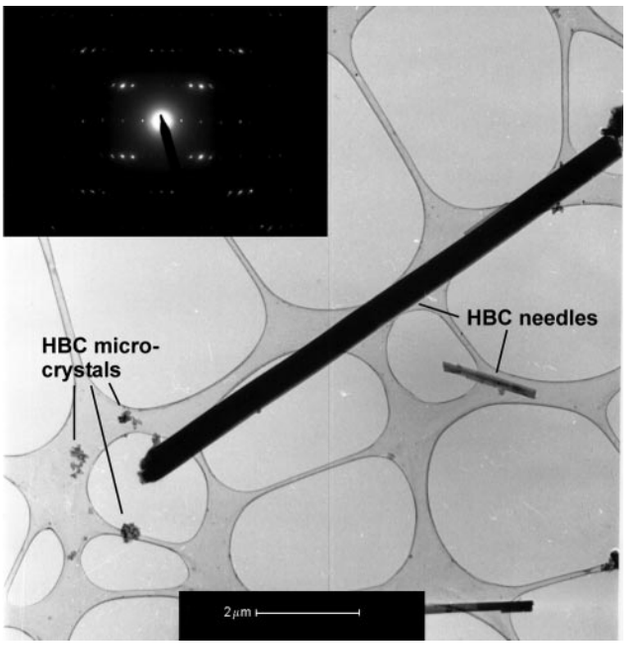

Fig. 7 TEM overview image of recrystallized HBC showing needles with different size and some remaining microcrystalline material. The inset shows a typical selected area electron diffraction pattern of one of the small needles.

structure in agreement with the one published for HBC **3** by Goddard *et al.*[14]

The combination of SAED and HREM shows that even though long, uniform needles with a crystal structure similar to the one known in the literature are formed,[14] the smaller crystals in particular exhibit many defects. In addition to a variation of the cell parameters a and c of the thin needles by about 10%, nearly all needle-like crystals are twisted around their long axis. Bend contours move more or less continuously over a distance of up to 200 nm indicating regular twisting of the needle (Fig. 8a). However, dark field images also indicate discontinuous twisting, probably mediated by small angle grain boundaries (Fig. 8b).

Some small microcrystallites also exhibit strongly bent lattice fringes (Fig. 9). In some extreme cases even concentric lattice fringes with a radius of curvature of about 2 nm were observed (Fig. 9b) around a central defect of about 3 to 4 molecules in diameter. The structural variations observed for the crystals and the high tendency for defect formation serve as an indication of a relatively flat energy surface as proposed by Gavezzotti and Desiraju for smaller PAHs.[7]

Heating HBC **3** to 480 °C led to sublimation of the material and large yellow needles ($0.1 \times 0.1 \times 0.5$ mm) were formed in the cold area (approx. 420 °C) of the sublimation ampoule. X-Ray diffraction analysis of these yellow single crystals ($a = 18.459$, $b = 5.122$, $c = 12.935$ Å, $\beta = 112.59°$, $P2_1/a$, $Z = 2$) showed that the structure is in good agreement with that of HBC **3** grown from molten pyrene by Goddard *et al.*[14] ($a = 18.431$, $b = 5.119$, $c = 12.929$ Å, $\beta = 112.57°$, $P2_1/a$, $Z = 2$).

Even at 480 °C some of the material did not sublime and formed brown needles ($0.03 \times 0.03 \times 0.1$ mm). The first suspicion that decomposition or oligomerization of the material had occurred could be falsified by laser desorption-time of flight mass spectrometry (LD-TOF MS) which showed an isotopically resolved spectrum of HBC. By using the residual powder mixture instead of the single crystals and suppressing all signals below 700 Da in the LD-TOF MS, traces of a HBC dimer could be observed, but the intensity of those signals was at the resolution limit indicating that the amount of this dimer is very small.

The occurrence of brown HBC crystals has been described by Goddard *et al.*[14] It is not clear to date whether this is a different polymorph. The small crystal size prevented a detailed crystal structure analysis. However, preliminary data suggest that we deal here with crystals of the already known HBC structure crystallizing in another crystal habit and presumably with a larger amount of lattice defects, *e.g.* stacking faults.

Owing to its lower molecular weight, DBPP **5** could be sublimed at lower temperatures than HBC **3**. Sublimation with a temperature gradient from 410 to 320 °C led to the formation of microcrystals between 320 and 370 °C whereas large needles ($0.1 \times 0.15 \times 2$ mm) as well as thin platelets (0.4×1.2 mm) were obtained between 370 and 410 °C. In the residual material, recrystallization with formation of both large needle-like crystals and thin platelets was observed.

The needle-shaped crystals of DBPP **5** obtained by

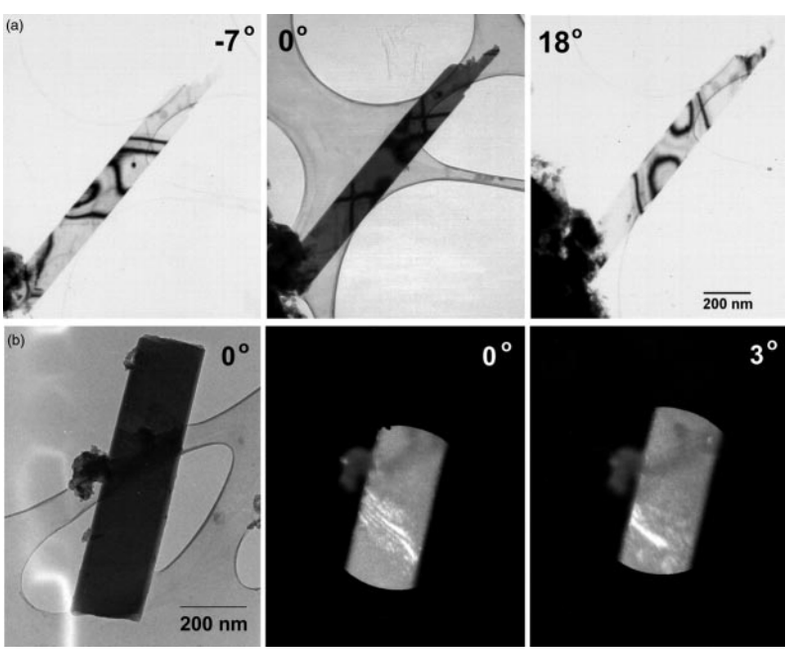

Fig. 8 (a) Bend contours in a twisted needle of HBC grown by heat treatment. During tilting the bend contours move continuously over a distance of up to 200 nm, before a sudden change is observed. (b) Bright field image and dark field images (310, 410, 510, 610 reflections) taken under a tilt angle difference of 3°.

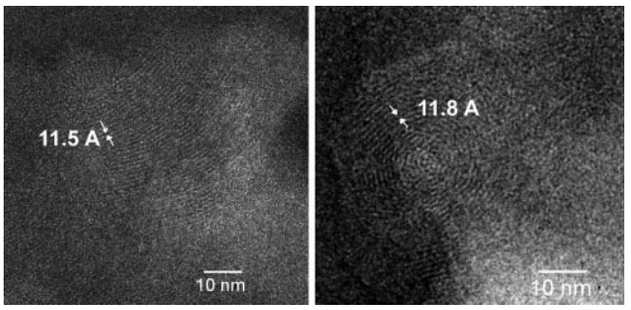

Fig. 9 Dislocations and strongly bent lattice fringes corresponding to the 001 plane.

sublimation had a sufficient quality for crystal structure determination (Fig. 10). DBPP **5** crystallizes in a herringbone-type structure (γ-motif) typical for large PAHs where the DBPP molecules are arranged in two columns with a tilt angle of 43° between the molecular plane and the stacking axis. This leads to an angle of 86° between molecules in neighboring columns along the *c* axis (Fig. 10a), whereas the molecules are oriented nearly parallel to each other along the *a* axis (Fig. 10b).

Two structural features of the crystal structure of DBPP **5** are especially noteworthy. One might expect that the "double-bay area", similar to the cove area, induces some slight distortion of the molecule, which would also explain the high solubility of DBPP **5** compared to that of HBC **3**. Nevertheless, structural analysis shows that DBPP **5** is nearly planar. The largest deviation of a carbon atom from the calculated best plane is 0.06 Å. This gives rise to a distance of the hydrogen atoms in the "double-bay area" of 1.97 and 1.98 Å (Fig. 11). The anisotropic thermal vibration ellipsoids show that, at least in the crystal, the main molecular motion is within the molecular plane. The anisotropic thermal motion of **5** can be described with good approximation as rigid body motion. TLS analysis[16] leads to eigenvalues of the root mean square librational amplitudes of 0.40, 2.78 and 5.68 degrees.[2]

An unusual structural feature is the packing of two neighboring DBPP molecules with the "double-bay areas" pointing towards each other, which generates a cavity with a diameter of about 4 Å between the molecules.[17] In the projection of the crystal structure approximately along the *b* axis (Fig. 10b) one recognizes that these cavities are not isolated, but form channels through the crystal.

At a first glance the formation of these channels is quite surprising. It might be anticipated that some small reorientation of the molecules along the *c* axis would close the cavities (Fig. 10b). However, this would only be true for a planar, graphite-like structure, but not for a herringbone-type structure. In the case of the γ-motif reorganization would lead to an interdigitation of neighboring stacks, which seems sterically impossible. Thus the strong tendency for the formation of a herringbone structure enforces the formation of channels.

The thin platelets which were also obtained by sublimation of DBPP **5** were too thin for a X-ray single crystal structure analysis, but the smallest platelets were of suitable dimensions to enable electron microscopic analysis. Examinations of about

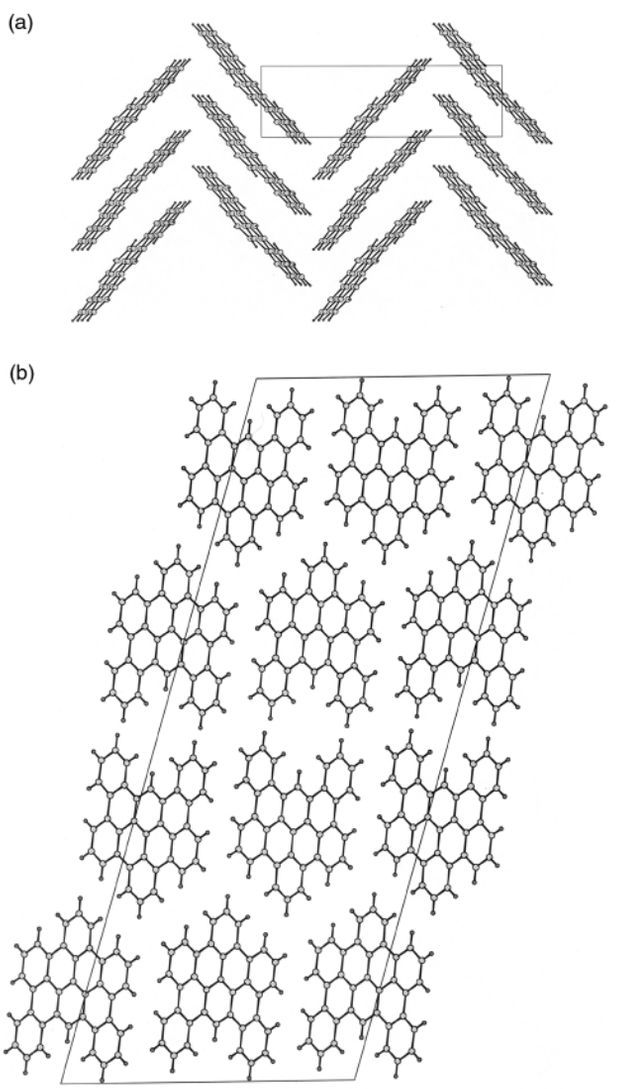

Fig. 10 Different projections of the crystal structure of DBPP **5**: (a) *b*–*c* plane, (b) *a*–*c* plane.

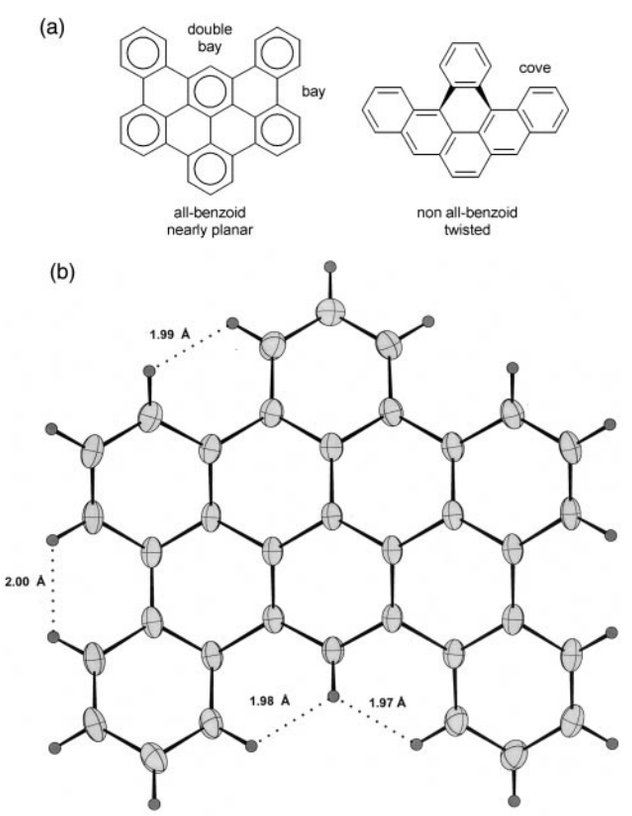

Fig. 11 (a) Influence of the topology: planar, all-benzoid structure of DBPP (**5**) containing bay and double-bay areas, and twisted structure of non-all-benzoid tribenzopyrene due to the cove area.[16] (b) Nearly planar geometry of a DBPP molecule **5** (with anisotropic thermal vibration ellipsoids according to crystal structure analysis at room temperature).

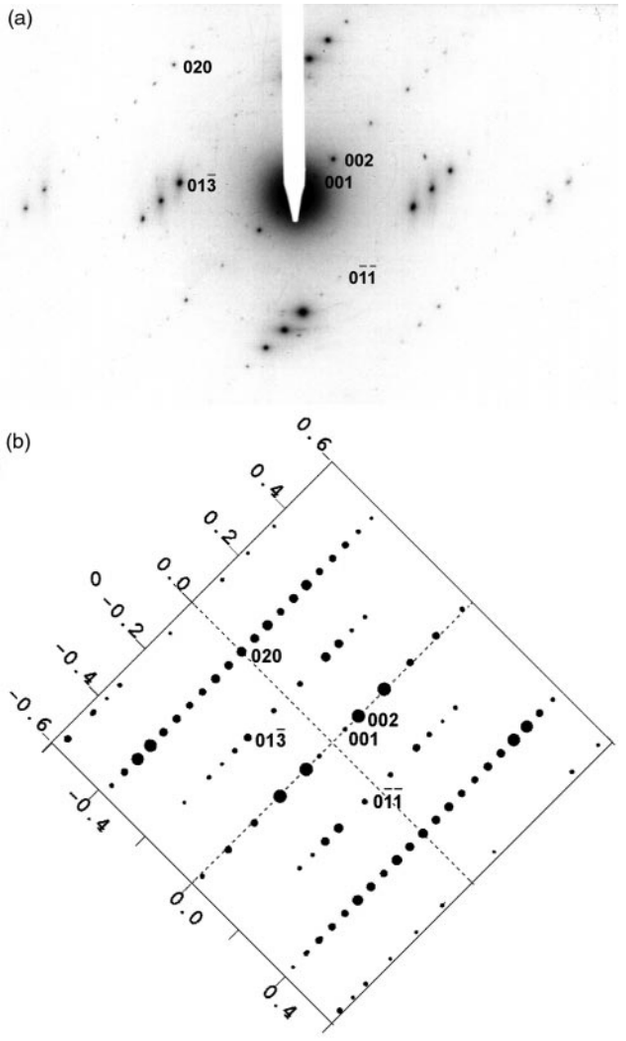

Fig. 12 (a) Selected area electron diffraction pattern of DBPP platelets. (b) Simulated[18] electron diffraction pattern of DBPP **5** (with $\alpha = 89^\circ$).

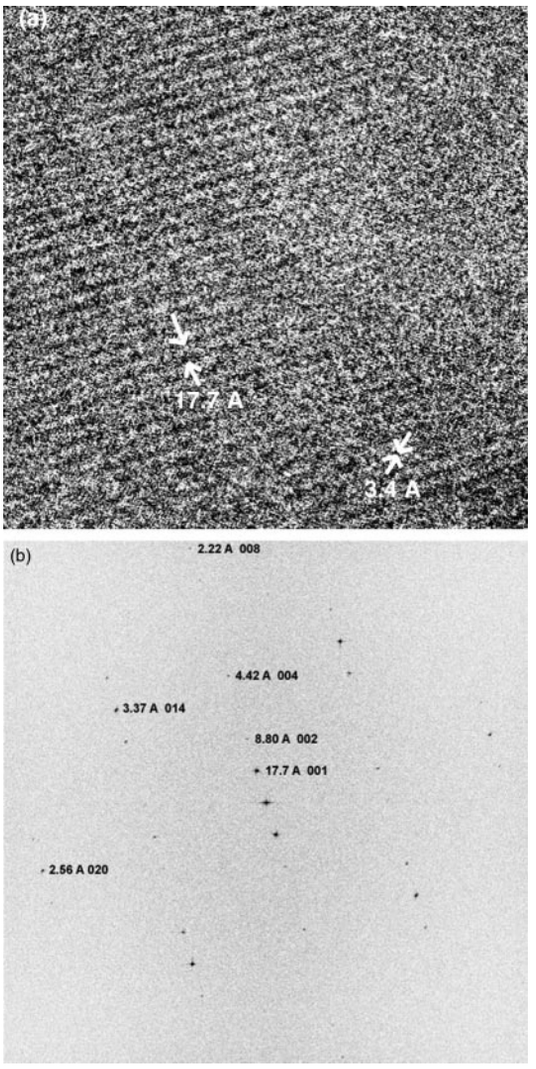

Fig. 13 (a) HREM image of DBPP **5**. (b) Fourier-transformed image[19] of the HREM micrograph.

thirty different crystallites by SAED showed the same zone for nearly all crystallites. The electron diffraction patterns (Fig. 12a) of those crystallites are essentially identical to the diffraction pattern of the [100] zone of the needle-shaped crystals shown above. The only difference is the angle α^*, which should be 90° for a monoclinic system, whereas approximately 89° was found by electron diffraction analysis. This effect may be due to a minor distortion of the crystal structure, presumably due to surface effects. Simulations[18] of the electron diffraction pattern using the structure of the needle-shaped crystals (slightly distorted with $\alpha = 89^\circ$) showed good agreement with the experimentally obtained diffraction pattern (Fig. 12). The lattice spacing and the systematic extinction of some reflections are the same, thus indicating only a small structural variation between the needles and the platelets.

The electron diffraction experiments indicated that the platelets have the same structure as that of the needle-shaped crystals. Furthermore, as most platelets are imaged with the [100] zone, this shows the *b*–*c* plane is the main growth direction. The platelets are very thin, which is consistent with the assumption that crystal growth in the direction of the "double-bay area" under formation of channels is less favorable than growth in the other two directions.

The stability of DBPP **5** under electron irradiation is high enough to also enable direct imaging of thin crystallites by low-dose high resolution electron microscopy. Fig. 13a shows a lattice image of DBPP **5** with the strongest observable lattice fringes corresponding to the 001 reflection. Several other lattice fringes are also visible with lower contrast. Fourier transformation[19] of the image (Fig. 13b) reveals that lattice fringes down to *d* spacings of 2.21 Å are present in the image. The *d* spacing, the intensities of the reflections and the systematic absence correspond to the diffraction pattern (Fig. 12). The only difference with the SAED pattern is the strong 100 reflection, which is only slightly visible in the diffraction pattern (Fig. 12). We suspect this effect to be due to the defocus of the image and the contrast transfer function modulating the observed intensities depending on the reciprocal spacing.

The HREM images of the sublimed DBPP **5** crystallites exhibit some crystal defects such as slight bending or insertion of lattice fringes, but in contrast to the heat-treated HBC sample these defects were observed only occasionally for the sublimed material. Furthermore, strongly bent lattice fringes as shown in Fig. 9 were never observed in the case of the sublimed crystals.

Conclusion

Synthesis of two large PAHs, hexabenzo[*bc*,*ef*,*hi*,*kl*,*no*,*qr*]coronene (HBC **3**) and dibenzo[*fg*,*ij*]phenanthro[9,10,1,2,3-*pqrst*]pentaphene (DBPP **5**), by oxidative cyclodehydrogention was shown to proceed smoothly starting from oligophenylene precursors by stepwise formation of new carbon–carbon bonds. The relatively high solubility of the intermediate product **2** as well as of DBPP **5** enabled, in addition to the

mass spectrometric and the UV/Vis-spectroscopic analysis, further NMR-spectroscopic support for the structure obtained. All analytical methods clearly indicate that intramolecular cyclodehydrogenation is the only reaction occurring under these oxidative reaction conditions.

The reaction products were originally partially crystalline to microcrystalline. By heat treatment at elevated temperatures it was possible to obtain well ordered materials. Recrystallization in the solid state leads to the formation of needle-shaped crystals from the originally microcrystalline material. However, these needle-like crystals still exhibit many defects.

At higher temperatures the PAHs can be sublimed using a temperature gradient to grow macroscopic single crystals. In case of HBC **3** sublimation led to the formation of needles, which crystallized in the γ-structure. Goddard *et al.* observed the same crystal structure by growth of HBC **3** from molten pyrene indicating that this packing pattern is thermodynamically very favorable.

By sublimation it was also possible to obtain single crystals of DBPP **5**, which crystallizes in the γ-motif. Owing to the "double-bay area" in the molecule channels of about 4 Å diameter are present through the crystal. Those channels could be used to insert other small molecules. Especially, the use of a doping reagent such as iodine to investigate its influence on the electronic properties of the material will be the topic of further experiments.

Experimental

Melting points were determined in open capillary tubes and are uncorrected. Argon was used for all preparations as an inert gas. Solvents and starting materials were purified according to standard procedures, when necessary. ^{1}H and ^{13}C NMR spectra were recorded using a Bruker DRX 500, mass spectra using a VG Instruments ZAB-2 and a Bruker Reflex-TOF. High-pressure liquid chromatography (HPLC) was carried out using a Kromail C8, 10 μm column with CH_3CN–CH_2Cl_2 as eluent (gradient starting with CH_3CN to CH_2Cl_2).

Preparations

Phenyldibenzo[*fg*,*ij*]phenanthro[9,10,1,2,3-*pqrst*]pentaphene 2. Copper(II) dichloride (4.84 g, 36.0 mmol) and aluminium(III) trichloride (4.80 g, 36.0 mmol) were stirred together with hexaphenylbenzene (**1**) (1.07 g, 2.00 mmol) in carbon disulfide (500 ml) under argon at room temperature for 12 hours before the reaction was quenched by addition of ethanol (500 ml). The suspension was filtered and the residue washed with dichloromethane (100 ml). The combined filtrates were dried under vacuum and the crude product containing **2** as well as hexaphenylbenzene (**1**) was purified twice by preparative HPLC. By slow evaporation of the solvent a few small crystallites of **2** were obtained before hexaphenylbenzene also precipitated. ^{1}H NMR (500 MHz, $C_2Cl_4D_2$, 353 K, ^{1}H–^{1}H COSY): δ 6.93 (2H, dd, H-h), 7.32 (2H, d, ^3J = 10.1, H-i), 7.44 (1H, dd, H-g), 7.49 (6H, m, H-j, H-k, H-l), 8.06 (2H, dd, H-d), 8.12 (1H, t, ^3J = 7.9, H-a), 8.61 (2H, d, ^3J = 8.1, H-f), 8.83 (2H, d, ^3J = 7.8, H-e), 8.96 (2H, d, ^3J = 7.9, H-c), 9.01 (2H, d, ^3J = 7.9, H-b). ^{13}C NMR (125 MHz, $C_2Cl_4D_2$, 353 K, J-mod): δ 121.35, 122.41, 122.51, 123.77, 124.64, 126.94, 127.18, 127.41, 127.87, 130.03, 131.32, 133.25 (*tert.-C*H), 121.07, 123.95, 125.17, 126.54, 130.24, 130.43, 130.81, 130.95, 132.36, 136.69, 145.14 (*quat.-C*). UV/Vis ($CHCl_3$): λ_{max} (log ε) = 311 (3.66), 324 (3.98), 338 (4.19), 368 (3.76), 383 (3.20), 411 (2.4), 421 (2.3), 435 (2.2); FD MS: *m*/*z* (%) 526 (M^+, 100).

Hexabenzo[*bc*,*ef*,*hi*,*kl*,*no*,*qr*]coronene (HBC) 3. Copper(II) dichloride (9.68 g, 72.0 mmol) and aluminium(III) trichloride (9.60 g, 72.0 mmol) were stirred together with hexaphenylbenzene (**1**) (1.07 g, 2.00 mmol) in carbon disulfide (500 ml) under argon for about two days at room temperature. When no remaining reactant was observed by mass spectrometry the reaction was quenched by addition of ethanol (500 ml). The suspension was filtered and the residue washed with H_2O, conc. HCl, H_2O, conc. amonia solution, H_2O, acetone, CS_2, CH_2Cl_2 (about 500 ml in small portions) and dried under vacuum. Yield: 1.0 g of HBC **3**. Sublimation was performed using a temperature gradient from 480 to 420 °C (over a range of 5 cm) at a pressure of 8×10^{-6} mbar. Mp > 300 °C. UV/Vis (1,2,4-trichlorobenzene): λ_{max} (log ε) = 343 (4.85), 359 (5.13), 387 (4.72), 399 (4.45), 420–450 (small aggregates). FD MS: *m*/*z* (%) 522 (M^+, 100). LD-TOF MS: *m*/*z* (%): 522 (M^+, 100). EDX: only carbon.

Dibenzo[*fg*,*ij*]phenanthro[9,10,1,2,3-*pqrst*]pentaphene (DBPP) 5. Copper(II) dichloride (584 mg, 4.36 mmol) and aluminium(III) trichloride (582 mg, 4.36 mmol) were stirred together with pentaphenylbenzene (**4**) (100 mg, 0.218 mmol) in carbon disulfide (80 ml) under argon for about two days at room temperature. When no remaining reactant was observed by mass spectrometry the reaction was quenched by addition of ethanol (50 ml). The suspension was filtered and the residue washed with H_2O, conc. HCl, H_2O, conc. amonia solution, H_2O, acetone, CS_2, CH_2Cl_2 (about 100 ml in small portions) and dried under vacuum. Yield: 95 mg of DBPP **5**. Sublimation was performed using a temperature gradient from 410 to 320 °C (over a range of 10 cm) at a pressure of 3×10^{-5} mbar. Mp > 300 °C. ^{1}H NMR (500 MHz, $C_2Cl_4D_2$, 353 K, ^{1}H–^{1}H COSY): δ 7.79 (2H, dd, H-d), 7.84 (2H, dd, H-c), 8.10 (3H, m, H-g, H-j), 8.84 (2H, d, ^3J = 8.0, H-e), 8.94 (2H, d, ^3J = 8.0, H-f), 9.05 (2H, d, ^3J = 8.1, H-h), 9.08 (2H, d, ^3J = 8.0, H-i), 9.14 (2H, d, ^3J = 8.1, H-b), 10.34 (1H, s, H-a). ^{13}C NMR (125 MHz, $C_2Cl_4D_2$, 353 K): δ 122.04, 122.32, 122.41, 124.17, 124.19, 124.23, 124.79, 127.14, 127.17, 127.25, 128.20, 128.25, 130.23, 130.44, 130.68, 130.71. UV/Vis ($CHCl_3$): λ_{max} (log ε) = 304 (4.70), 318 (4.65), 333 (4.77), 363 (4.46), 375 (4.16), 405 (3.65), 414 (3.59), 429 (3.45). FD MS: *m*/*z* (%) 450 (M^+, 100), 225 (M^{2+}, 25). EDX: only carbon.

Crystal structure determination

The crystal structure of DBPP **5** was determined at room temperature on a Nonius CAD4 diffractometer with graphite monochromated Cu-Kα radiation (λ = 1.5418 Å). The lattice parameters were obtained by a least square analysis of the setting angles of 25 reflections with θ > 20°. The structure was solved by direct methods (SIR 92)[20] and refined by full-matrix least squares analysis with anisotropic thermal parameters for the carbon atoms. The hydrogen atoms were placed according to the binding geometry and refined with fixed isotropic thermal parameters in the riding mode. 4011 Reflections, 2112 observed ($I > 3\sigma(I)$), empirical correction; refinement on *F*; unit weight; $R = 0.047$, $R_w = 0.057$. Monoclinic, space group *C*2/*c*, $a = 45.381(1)$, $b = 5.1771(7)$, $c = 18.266(1)$, $\beta = 106.293(6)°$, $V = 4110.1$ Å^3, $Z = 8$, $D_x = 1.453$ g cm^{-3}.

CCDC reference number 1145/206.

See http://www.rsc.org/suppdata/jm/a9/a90841a for crystallographic files in .cif format.

Acknowledgements

This work was supported by the Volkswagen Stiftung and the Bundesministerium für Bildung und Forschung (BMBF). We thank Dr J. Räder and Dipl. Chem. K. Martin for the LD-TOF MS measurements and Dr C. Honecker for his help with the sublimation of DBPP. C.K. thanks the BMBF and Fonds der Chemischen Industrie for a scholarship.

References

1 R. Scholl, C. Seer and R. Weitzenböck, *Chem. Ber.*, 1910, **43**, 2202; R. Scholl and C. Seer, *Liebigs Ann. Chem.*, 1912, **55**, 111; R. Scholl and H. Neumann, *Chem. Ber.*, 1922, **55**, 118.

2 E. Clar and D. G. Stewart, *J. Am. Chem. Soc.*, 1953, **75**, 2667; E. Clar, C. T. Ironside and M. Zander, *Tetrahedron*, 1966, **22**, 3527; E. Clar and W. Schmidt, *Tetrahedron*, 1979, **35**, 2673.

3 M. Zander, *Chem. Ber.*, 1962, **92**, 2749; M. Zander and W. H. Franke, *Angew. Chem.*, 1964, **76**, 922; *Angew. Chem., Int. Ed. Engl.*, 1964, **3**, 755.

4 E. Clar, *The Aromatic Sextet*, John Wiley and Sons, London, 1972.; H. Hosoya, *Top. Curr. Chem.*, 1990, **153**, 255; M. Zander, *Polycyclische Aromaten: Kohlenstoffe und Fullerene*, B. G. Teubner, Stuttgart, 1995.

5 (*a*) S. E. Stein and R. L. Brown, in *Molecular Structure and Energetics*, VCH-Verlag, Weinheim, 1987, vol. 2; (*b*) S. E. Stein and R. L. Brown, *J. Chem. Soc.*, 1958, 1861.

6 H. Marsch and M. A. Diez, in *Liquid Crystalline and Mesomorphic Polymers*, eds. V. P. Shibaev and L. Lam, Springer-Verlag, New York, Berlin, 1993; A. Oberlin, in *Chemistry and Physics of Carbon*, ed. P. A. Thrower, Marcel Dekker Inc., New York, Basel, 1989, vol. 22.

7 A. Gavezzotti and G. R. Desiraju, *Acta Crystallogr., Sect. B*, 1988, **44**, 427; G. R. Desiraju and A. Gavezzotti, *Acta Crystallogr., Sect. B*, 1989, **45**, 473.

8 V. S. Iyer, M. Wehmeier, J. D. Brand, M. A. Keegstra and K. Müllen, *Angew. Chem.*, 1997, **109**, 1675; *Angew. Chem., Int. Ed. Engl.*, 1997, **36**, 1603; M. Müller, J. Petersen, R. Strohmeier, C. Günther, N. Karl and K. Müllen, *Angew. Chem.*, 1996, **108**, 947; *Angew. Chem., Int. Ed. Engl.*, 1996, **35**, 886.

9 (*a*) E. Clar, C. T. Ironside and M. Zander, *J. Chem. Soc.*, 1959, 142; (*b*) E. Clar and M. Zander, *J. Chem. Soc.*, 1958, 1861; (*c*) A. Halleux, R. H. Martin and G. S. D. King, *Helv. Chim. Acta*, 1958, **129**, 1177.

10 The AM1 structure optimization was performed using Spartan 4.0 by Wavefunction Inc., Irvine, CA, starting with a planar central aromatic core and the free phenyl ring orthogonal to it as well as at an angle of 45°.

11 R. A. Pascal, Jr., W. D. McMillan, D. Van Engen and R. G. Eason, *J. Am. Chem. Soc.*, 1987, **109**, 4660.

12 C. Kübel, Ph.D. thesis, Johannes Gutenberg-University, Mainz, Germany, 1998.

13 The electron microscopic analysis was performed using a Philips CM12 microscope equipped with a LaB_6 cathode operating at 120 kV in low-dose mode at nominally 60 000 times magnification. The electron diffraction patterns were calibrated with TlCl and the measurements done with a selected area aperture of 40 μm. The high-resolution images were calibrated using a grid with 2160 lines per mm. The samples were prepared by ultrasonication of the PAH in methanol. After precipitation of the larger crystals the remaining dispersion was sonicated again and the dispersion dried on a copper grid covered with amorphous carbon film.

14 R. Goddard, M. W. Haenel, W. C. Herndon, C. Krüger and M. Zander, *J. Am. Chem. Soc.*, 1995, **117**, 30; J. M. Robertson and T. Trotter, *J. Chem. Soc.*, 1961, 1280.

15 Ampoules with a diameter of 2 cm and a length of about 5 or 10 cm were used for the sublimation. 20 to 50 mg of the PAH were inserted and the sample heated to 200 °C at a vacuum of 10^{-2} mbar for 2 hours. Afterwards the ampoule was closed under a vacuum of about 10^{-5} mbar. A self-made oven which was heated on one side was used for the sublimation. The temperature gradient was calibrated with a thermal element.

16 V. Schomaker and K. N. Trueblodd, *Acta Crystallogr., Sect. B*, 1968, **24**, 63.

17 The size of the channel was determined as the distance between atomic centers of hydrogen atoms on opposite sides of the cavity with twice the van der Waals radius for hydrogen subtracted.

18 The electron diffraction pattern was simulated using the crystal diffraction module of the program Cerius^2 Version 3.5 by Molecular Simulations Inc.

19 The Fourier transformation was performed using the program Analysis 2.11 by Soft-Imaging GmbH.

20 SIR 92, *J. Appl. Crystallogr.*, 1994, **27**, 435.

Paper a908941a